Applied Catalysis B: Environment and Energy 347 (2024) 123791

Contents lists available at ScienceDirect

Applied Catalysis B: Environment and Energy

journal homepage: www.elsevier.com/locate/apcatb

Rhenium redefined as electrocatalyst: Hydrogen evolution efficiency boost via Pt and Ni doping

Jinho Kim [a], Jongwon Oh [b], Sambath Baskaran [c], Tae Gyun Kim [c], Soyoung Kim [e], Jieun Yang [d,*], Jaehoon Jung [c,*], Seok Min Yoon [a,*]

[a] Department of Chemistry, Gyeongsang National University, Jinju 52828, Republic of Korea
[b] Department of Chemistry, Wonkwang University, 460 Iksandae-ro, Iksan, Jeonbuk, Republic of Korea
[c] Department of Chemistry, University of Ulsan, Ulsan 44610, Republic of Korea
[d] Department of Chemistry, College of Science, Kyung Hee University, 26 Kyungheedae-ro, Dongdaemun-gu, Seoul 02447, Republic of Korea
[e] Analysis and Assessment Group, Research Institute of Industrial Science and Technology, Pohang 37673, Republic of Korea

ARTICLE INFO

Keywords:
Rhenium
Hydrogen evolution reaction
Electrocatalysis
Nanoparticle clusters
Transition metal doped catalysts
Alkaline water electrolysis

ABSTRACT

Rhenium metal-based catalysts are potential candidates to imperatively replace precious platinum catalysts for green hydrogen production via the hydrogen evolution reaction (HER) in water electrolysis. Theoretically, the electrocatalytic HER activity of Re is comparable to that of the platinum group metals (PGMs). In addition, Re is more cost-effective than the noble PGMs. Herein, tiny amount of Pt- and Ni-doped Re nanoparticle clusters interconnected by amorphous carbon (Pt-Ni@Re/C NPCs) are successfully synthesized to improve the HER catalytic activity of Re metal. Pt-Ni@Re/C NPCs achieved phenomenally enhanced electrocatalytic HER performance in both acidic and alkaline media. Pt-Ni@Re/C NPCs exhibit a particularly superb performance in alkaline media regarding low overpotential, Tafel slope, and excellent stability, which is superior or comparable to that of Pt-based catalysts. Therefore, the newly designed Pt-Ni@Re/C NPCs is a promising candidate as a HER electrocatalyst to boost the developing industrial green hydrogen production system.

1. Introduction

Water electrolysis is an ideal method of producing environmentally clean hydrogen with zero emission of carbon-containing pollutants [1,2]. Despite its potential, there are two major obstacles impeding the production of industrial H_2 through water electrolysis. The first obstacle involves the heavy reliance of most well-developed electrolysis systems on precious platinum group metals (PGMs) due to their superior electrocatalytic performance [3–6]. The second challenge relates to the operational characteristics of most technically mature hydrolysis systems, which predominantly use alkaline water electrolyzers [7]. While alkaline water electrolysis benefits from a diverse range of non-precious electrocatalysts for oxygen evolution reactions (OER) [8], it is hindered significantly by the sluggish kinetics of the cathodic hydrogen evolution reaction (HER) in alkaline electrolytes [9]. This limitation underscores the importance of identifying novel catalysts that can enhance HER efficiency in alkaline environments, a development that could substantially advance practical and industrial hydrogen production.

As such, Re-based nanocatalysts can be attractive substitutes for the PGMs in electrocatalytic HER for the following reasons: i) Re can potentially promote very active electrocatalytic HER similar to PGMs, under acidic and alkaline conditions, because Re is located near to the PGMs in the volcano plot (Fig. 1a) [1,10], which illustrates the theoretical estimation of electrocatalytic HER potential of various metals [11]. ii) Re nanoparticles can exhibit efficient electrocatalytic HER and Re is very stable under universal pH conditions in acidic and alkaline media [12]. iii) Re is much more economical than PGMs. The cost of Re is approximately 3–7% of that of Pt, based on market fluctuations [13]. As of 2023, the price of Re is 3% of that of Pt [14]. Nevertheless, Re-only-based catalysts have not practically presented electrocatalytic HER performance comparable to the PGMs. Therefore, despite catalytic advantages, Re-based electrocatalysts for HER have received relatively little attention compared to other catalysts.

Recently, Re-based HER electrocatalysts have garnered increasing interest, largely owing to the previously highlighted advantages of Re [10,15]. Notably, Re is a promising alternative for splitting water under universal pH conditions. Nevertheless, at lower pH, metallic Re can potentially form rhenium hydride $Re + e^- \rightarrow ReH$) as indicated by its

* Corresponding authors.
E-mail addresses: jey@khu.ac.kr (J. Yang), jjung2015@ulsan.ac.kr (J. Jung), seokminyoon82@gmail.com (S.M. Yoon).

https://doi.org/10.1016/j.apcatb.2024.123791
Received 21 September 2023; Received in revised form 12 January 2024; Accepted 28 January 2024
Available online 30 January 2024

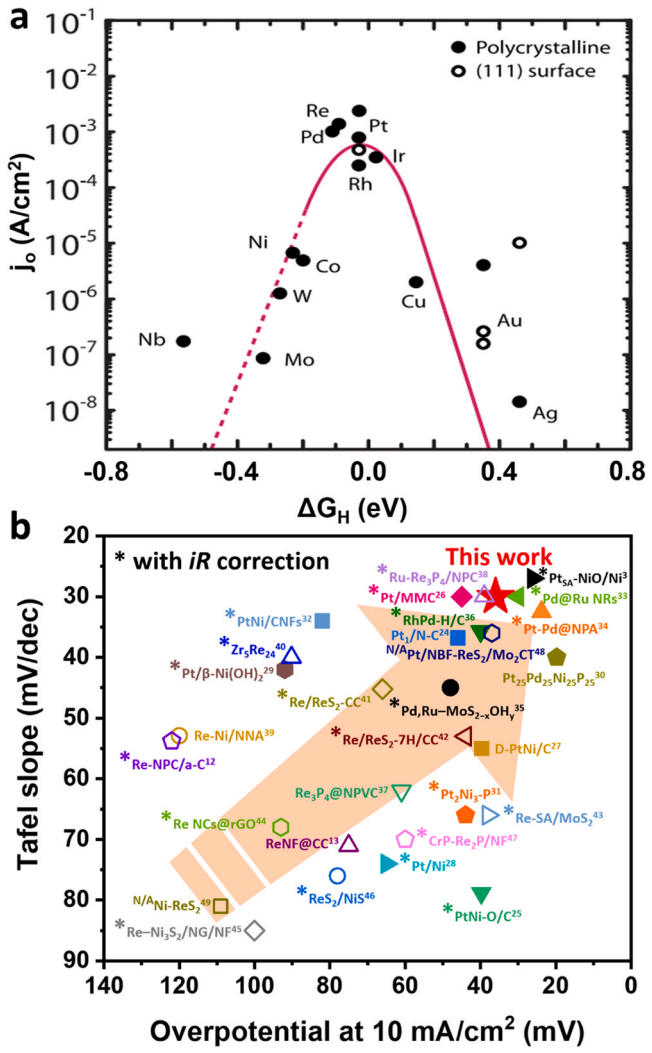

Fig. 1. Theoretical potential of Re as an efficient electrocatalyst for HER and experimentally measured superior electrocatalytic HER performance of Pt-Ni@Re/C NPCs in alkaline media. (a) HER volcano plot for metals. Adapted and modified with permission from (Ref. 1). (b) Comparative analysis of the HER performance of Pt-Ni@Re/C NPCs and Re-based and PGMs-based electrocatalysts in 1 M KOH. The asterisk (*) denotes electrocatalysts that displayed the Tafel slope and overpotential with *iR* correction, whereas the absence of the asterisk shows the results obtained without *iR* correction. Detailed information regarding Tafel slope and overpotential is provided in Table S1. Superscripts at each catalyst denotes references.

Pourbaix diagram, a condition that could potentially overestimate HER on metallic rhenium [11]. In contrast, half-reactions involving metallic Re, such as disproportionation, become negligible above pH 6. As such, Re could be a more suitable electrocatalyst for HER under alkaline conditions than under acidic conditions. Notwithstanding, to make a substantial impact, further enhancement of HER activity and commercial applicability of metallic Re-based catalysts is required. Additionally, a deep dive into the inherent reasons for Re's catalytic proficiency in HER remains overdue.

To improve the electrocatalytic HER activity of Re, other transition metals (TMs) need to be incorporated into the Re metal, giving rise to the consideration of Re-based alloys such as TM–Re (TM = Au, Pd, Pt, Ir, Ru, Co, Fe, Ni, etc.), which are known to be efficient heterogeneous catalysts for the hydrogenation reaction [16]. For example, Pt–Re is regarded as an essential catalyst in petroleum refinery processes to produce high-octane lead-free gasoline by hydrogenating unsaturated hydrocarbon [17,18]. Ir–Re, Pd–Re, and Ni–Re catalysts have performed well in heterogeneous catalytic hydrogenation of carboxylic acid and carbonyls [19]. The efficient hydrogenation catalysis of Re alloys implies that a combination of Re and TMs can facilitate more intimate interaction with hydrogen.

A minuscule amount of Pt and Ni (5 mol% each) are imposed into Re nanoparticle clusters (NPCs), an aggregated form of interconnected nanoparticles with amorphous carbon (Pt-Ni@Re/C NPCs), to enhance the electrocatalytic HER activity of Re. The fused Ni stably forms NiO, NiOOH, and $Ni(OH)_2$ under alkaline conditions, which develop oxophilic sites, thus promoting the Volmer step ($H_2O + M + e^- \rightarrow MH^* + OH^-$), where M denotes the metal and H* denotes an adsorbed hydrogen on the surface of an electrocatalyst [20,21]. In addition, merged Pt aids the adsorption of hydrogen and the reduction of protons [22]. Furthermore, Re can have a more partial positive charge (δ^+) when Pt and Ni are adjacent to Re because of its relatively low electronegativity (1.91) compared to those of Pt (2.28) and Ni (1.93), which may facilitate the Volmer reaction process by water molecule adsorption and dissociation [20,23]. As a result, Pt-Ni@Re/C NPCs efficiently dissociate H_2O and exhibit higher electrocatalytic HER performance than Pt/C, which is a representative HER catalyst under alkaline media. Even when compared to recently reported efficient HER catalysts under alkaline conditions, the Pt-Ni@Re/C NPCs exhibit exceptional performance, establishing themselves as excellent catalysts for hydrogen production (Fig. 1b and Table S1) [3,12,13,24–49]. This is illustrated by their lower overpotential (η_{10} = 36 mV, η_{10}: overpotential at 10 mA cm^{-2}), Tafel slope (30 mV dec^{-1}) and activation energy (16.2 kJ mol^{-1}) compared to those of Pt/C. Pt-Ni@Re/C NPCs also possess a low overpotential (419 mV) at a high current density (1000 mA cm^{-2}: η_{1000}) in alkaline media. The performance of electrocatalysts at large current densities is critical for industrial uses [50,51]. Also, Pt-Ni@Re/C NPCs exhibit excellent durability under alkaline media due to the remarkable thermal and chemical stabilities of Re. Moreover, the Faradaic efficiency of this catalyst for HER exhibited 98.63%, which value is nearly 100%. Further, turnover frequency (TOF) for the electrocatalytic HER at exchange current density was 0.12 s^{-1}. Herein, carbon monoxide stripping tests, underpotentially detected hydrogen (H_{upd}), and density functional theory (DFT) studies corroborate that water molecules can dissociate on the Pt-Ni@Re/C NPCs surface under high pH conditions more efficiently than Pt/C. These results suggest that metallic Re-based nanoparticles can be novel catalysts for HER as alternatives to PGMs-based catalysts and thereby strongly contribute to industrial green hydrogen production by electrocatalytic water splitting.

2. Experimental section

Chemicals, synthesis of Pt@Re/C, Ni@Re/C, Re/C NPCs, characterization, and computational methods are presented in Supplementary Materials.

2.1. Synthesis of Pt-Ni@Re/C NPCs

First, 0.192 g Re_2O_7, 0.008 g $Pt(acac)_2$, 0.005 g $Ni(acac)_2$, and 1 mL of THF were put into a 20 mL glass vial. A gel was formed when the mixture was gently shaken and left at ambient conditions for 24 h. One gram of gel was dissolved in pure THF and then heated at 250 °C in a furnace for 2.5 h. Then, the powder was washed 5 times with pure THF, and each washing step, which lasted for 10 min, included centrifugation at 10,000 rpm. Last, to synthesize Pt-Ni@Re/C NPCs, 10 mg of the product was annealed to 500 °C in an Ar or mixture of hydrogen and argon (H_2: Ar = 5: 95) for 4 h at a heating rate of 5 °C min^{-1}. All annealing processes were conducted with a gas flow rate of 200 sccm.

2.2. Electrochemical measurements

All electrochemical data were recorded by IVIUMnSTAT (Ivium Technologies). A three-electrode system was used to conduct the

experiment: a glassy carbon (GC) rotating disk electrode, glassy carbon plate, and Nickel foam (NF) were used as working electrodes, and a graphite rod was used as a counter electrode. For the reference electrodes, Ag/AgCl (in 3 M NaCl solution) and Hg/HgO (in 1 M NaOH solution) were used under acidic and alkaline conditions, respectively. The reference was calibrated against and converted to a reversible hydrogen electrode (RHE). To make ink solutions, 4 mg of catalysts were dispersed in a 1 mL of water and ethanol mixed solution ($V_{water}/V_{ethanol}$ = 3/1) with 40 μL of 5 wt% Nafion solution and sonicated for 30 min. Then, 5 μL of catalyst ink was loaded onto the GC electrode (diameter: 3 mm) and dried in ambient conditions. The resulting catalyst loading was 0.283 mg cm^{-2}. Before all electrochemical measurements, the electrolytes were purged with N_2 or Ar gas for 30 min and CV was scanned 20 times at a rate of 100 mV s^{-1} until stable. Owing to the design of the GC-RDE (glassy carbon-rotating disk electrode), the catalyst-loaded electrode surface is immersed in the electrolyte, oriented downwards. This positioning often leads to the adherence of undesired air bubbles on the electrode surface. To counteract this issue effectively, we implement 20 CV (cyclic voltammetry) cycles prior to taking measurements. Unless otherwise noted, polarization curves were measured at the scan rate of 2 mV s^{-1}. The electrochemically active surface area (ECSA) estimated the double-layer capacitance by measuring it in potential regions without a Faradaic current feature. To estimate the double layer capacitance (C_{dl}), CVs were obtained at six different scan rates of 10, 20, 40, 60, 80, and 100 mV s^{-1} at a potential range of 0.1–0.2 V vs. RHE. EIS analyses were performed at an overpotential of − 0.2 V vs. RHE. from 100 kHz to 10 mHz in 1 M KOH and with an alternating current amplitude of 5 mV. Two experiments were conducted to verify the stability of the catalyst. For cycling experiments, the potentials ranging from 0.1 to − 0.5 V were compared with the initial data after 10,000 CV scans. Additionally, an overpotential of − 0.5 V was provided for 48 h and the resulting change in current density was obtained. The relevant experiment was conducted several times and the error bar was obtained by excluding the maximum and minimum values. A CO-saturated 1 M KOH solution was prepared for the carbon monoxide (CO) stripping tests. CO_{ad} was subsequently generated on the catalyst surface under this electrolyte, and dissolved CO in the electrolyte was subsequently removed using pure Ar gas. Following all the necessary preparations, CV curves were acquired.

3. Results and discussions

3.1. Synthesis and structural characterizations of Pt-Ni@Re/C NPCs

Pt-Ni@Re/C NPCs were synthesized using the following three steps: (i) Rhenium oxide-polytetrahydrofuran (ReO_x −PTHF) gel composite was prepared by dissolving 0.4 mM of Re_2O_7 in tetrahydrofuran (THF) solvent, and left for 24 h under ambient conditions. To synthesize Pt-

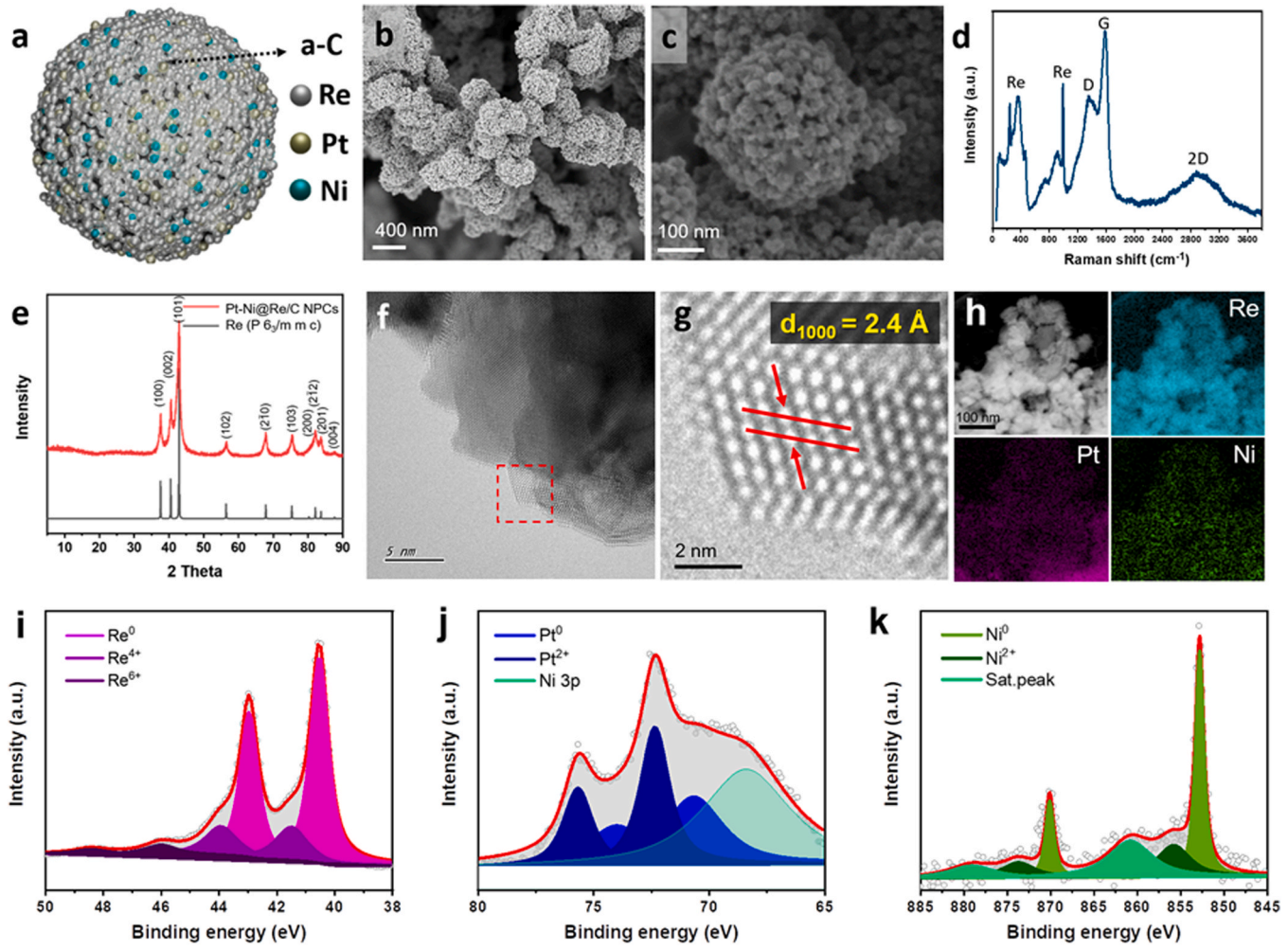

Fig. 2. Structural characterization of Pt-Ni@Re/C NPCs. (a) Schematic illustration of Pt-Ni@Re/C NPCs. SEM images of Pt-Ni@Re/C NPCs with (b) low magnification and (c) high magnification. (d) Raman spectra of the Pt-Ni@Re/C NPCs. (e) PXRD pattern of Pt-Ni@Re/C NPCs. (f) Low-magnified, and (g) high-magnified HR-TEM images of Pt-Ni@Re/C NPCs. (h) HAADF image of Pt-Ni@Re/C NPCs and EDS mapping results for scanning for Re, Pt, and Ni. (i) 4 f XPS spectra of Re. (j) 4 f XPS spectra of Pt. (k) 2p XPS spectra of Ni.

Ni@Re/C NPCs, a small quantity (5 mol%) of platinum (II) acetylacetonate ($Pt(acac)_2$) and nickel (II) acetylacetonate ($Ni(acac)_2$) were dissolved with Re_2O_7 precursor powder in THF. The gelation was proceeded by spontaneous cationic ring-opening polymerization of monomeric THF with strong Lewis acidic Re_2O_7 [12,52,53]. (ii) The blended ReO_x-PTHF gel with a tiny amount of $Pt(acac)_2$ and $Ni(acac)_2$ produced a black powder of Pt-Ni@ReO_x/C NPCs after solvothermal processing in an autoclave for 2.5 h at 250 °C. (iii) Finally, to further reduce Pt-Ni@ReO_x/C NPCs and the surface oxides of Re, Pt-Ni@ReO_x/C NPCs were annealed at 500 °C under H_2/Ar mixed gas environment with a gas flow rate of 200 sccm for 4 h to produce Pt-Ni@Re/C NPCs (Fig. 2a-c; Experimental section).

Scanning electron microscope (SEM) images show that berry-type clusters possess an average diameter of 400 nm (Fig. 2b-c), and the clusters consist of densely interconnected nanoparticles which an average diameter of 25 nm (Fig. S1). The nanoparticles held each other with amorphous carbon (a-C), characterized by the detection of D (1368 cm^{-1}) and G (1580 cm^{-1}) bands in Raman spectroscopy (Fig. 2d), which indicates the formation of *a*-C [12]. Powder X-ray diffraction (PXRD) revealed that the final product displays a metallic Re crystal structure with a hexagonal unit cell and $P6_3/mmc$ space group ($a = b =$ 2.76 Å, $c =$ 4.46 Å, $\alpha = \beta = 90°$, $\gamma = 120°$) (Fig. 2e) [54]. The PXRD patterns of the Pt-Ni@Re NPCs only display the metallic crystalline structure of Re, rather than Pt and Ni, which implies that a small amount of Pt and Ni randomly fused into the Re metal surface.

High-angle annular dark field scanning transmission electron microscopy (HAADF-STEM) and energy-dispersive X-ray spectroscopy (EDS) directly prove that the a-C interconnecting the nanoparticles as well as Pt and Ni were dispersed at the surface of the Re nanoparticles. (Fig. 2h) and the relative contents of Pt and Ni are 7.33% and 0.62%, respectively, compared to Re (Fig. S2). High-resolution transmission electron microscopy (HR-TEM) revealed that the nanoparticles possess a monocrystal character that exhibits spacings of 2.40 Å between the plane (1000) on zone plane (0001) (Fig. 2f-g).

X-ray photoelectron microscopy (XPS) verified the presence of each metal and the oxidation states in Pt-Ni@Re/C NPCs (Fig. 2i-k). The XPS displays distinct peaks of Re from 38 eV to 50 eV [54,55], which are subsequently deconvoluted. As a result, peaks at 40.73 eV and 43.16 eV are associated with fully reduced metallic Re (Re 4 $f_{7/2}$ and Re 4 $f_{5/2}$), and peaks at 41.67 eV and 44.13 eV, 46.2 eV, and 48.63 eV are attributed to Re^{4+} and Re^{6+} generated by surface oxidation (Fig. 2i) [56]. Importantly, compared to the synthesized Re-NPC/a-C in the absence of Pt and Ni, the Re^0 4 f peak was clearly positively shifted (Fig. S3). In addition, Pt 4 f spectra was observed from 64 eV to 80 eV, which are attributed to Pt^0 (70.67 eV and 74 eV) and Pt^{2+} (72.35 eV and 75.68 eV) (Fig. 2j) [57]. The incorporated Ni exhibits two oxidation states (Ni^0 (852.8 eV and 870.1 eV), Ni^{2+} (855.8 eV and 873.7 eV), and sat. peak (860.8 eV and 879.1 eV)) in Pt-Ni@Re/C NPCs (Fig. 2k) [58]. Noticeably, the peaks related to Pt 4 f and Ni 2p displayed significantly negative shifts compared to those of commercial Pt/C, PtNi/SWNT, and metal-doped Pt_3Ni/C nanoparticles [59,60]. The negative shift might result from the strong electron transfer that occurred from Pt and Ni particles because of the relatively lower electronegativity of Re than Pt and Ni, which indicate that the Pt and Ni are inserted into the Re surface in Pt-Ni@Re/C NPCs.

3.2. Electrocatalytic HER performance of Pt-Ni@Re/C NPCs

The electrocatalytic HER activities of Pt-Ni@Re/C NPCs were investigated by measuring polarization curves obtained by linear scan voltammetry (LSV, scan rate: 2 mV s^{-1}) using a working electrode prepared by loading the NPCs ink on a glassy carbon rotating disk (mass loading: 0.283 mg cm^{-2}) (see the methods in the Supplementary Materials). Fig. 3 shows the electrocatalytic HER performances of Pt-Ni@Re/C NPCs and other analogous Re/C NPCs under alkaline media (pH 14). The monometallic Re/C NPCs without transition metal dopants displayed electrocatalytic HER activity similar to that in a previous report [12]. The Re/C NPCs exhibited overpotential of 136 mV at

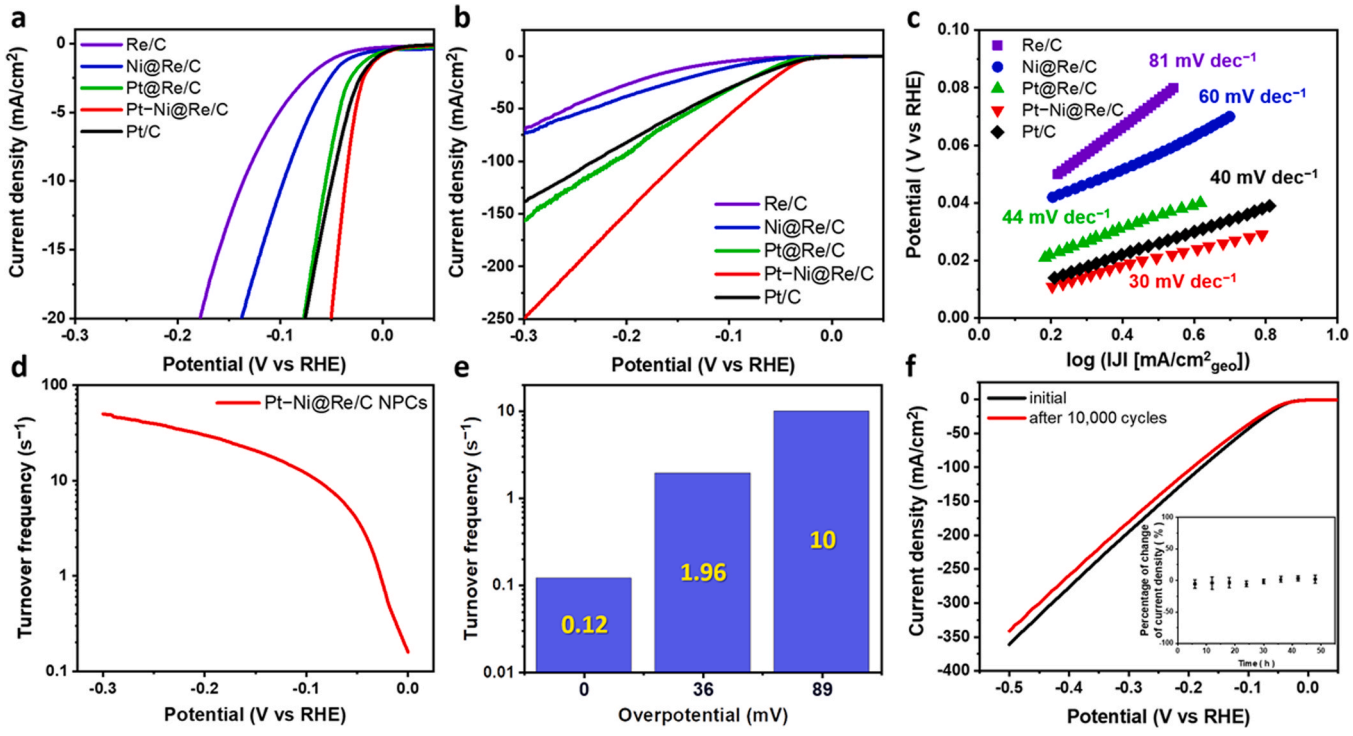

Fig. 3. Electrocatalytic performance of Pt-Ni@Re/C NPCs for the HER. (a and b) LSV curves of Re/C, Ni@Re/C, Pt@Re/C, Pt-Ni@Re/C NPCs, and Pt/C in 1 M KOH electrolyte. (c) Tafel slopes for each HER electrocatalyst as shown in (a). (d) TOF values of the Pt-Ni@Re/C NPCs. The plot was obtained from (b). (e) TOF value corresponding to typical overpotential. (f) LSV curves of Pt-Ni@Re/C NPCs before (black curve) and after (red curve) 10,000 HER cycles. The inset displays the average current density change at − 500 mV vs RHE for 48 h; This stability test was repeated 5 times.

10 mA cm^{-2} (η_{10}), and the Tafel slope was 81 mV dec^{-1} (Fig. 3a-c). The Tafel slope is derived from the LSV curve. On the other hand, transition metal-doped Re/C NPCs (Pt@Re/C, Ni@Re/C, and Pt-Ni@Re/C NPCs) exhibited enhanced catalytic activity. Significantly, the Pt-Ni@Re/C NPCs outperformed electrocatalytic HER performance, which was comparable to that of Pt/C under acidic conditions, yielding a low η_{10} of 49 mV and Tafel slope of 29 mV dec^{-1} (Fig. S4). Noticeably, the Pt-Ni@Re/C NPCs presented lower η_{10} (36 mV) than commercial Pt/C (49 mV) under alkaline conditions (Fig. 3a), although the η_{10} was not ohmic resistance (*i-R*) corrected. Further, the Pt-Ni@Re/C NPCs exhibited the fastest kinetics with the Tafel slope of 30 mV dec^{-1} compared to the Pt/C, Ni@Re/C, Pt@Re/C, and Re/C NPCs, although sluggish kinetics generally occurred under alkaline conditions. Interestingly, Pt-Ni@Re/C NPCs provided a higher current than Pt/C at the same overpotential (300 mV vs. RHE), resulting in vigorous evolution of hydrogen gas from the Pt-Ni@Re/C NPCs deposited glassy carbon plate (Fig. S5).

The electrocatalytic HER performances of Re/C NPCs were compared with those of Pt-Ni@Re/C NPCs under acidic (Fig. S4) and alkaline media (Fig. 3a-c). The binary metallic systems yielded better HER activity than the Re/C NPCs in both media, but the activity parameters were still lower than those of Pt-Ni@Re/C NPCs and Pt/C. In the electrocatalytic reaction under alkaline conditions, the η_{10} values of Ni@Re/C and Pt@Re/C NPCs are 97 and 55 mV, respectively (Fig. 3a). The Tafel slopes are 60 and 44 mV dec^{-1} for Ni@Re/C and Pt@Re/C NPCs, respectively (Fig. 3c). Therefore, the control experiment reveals that tertiary metallic systems such as Pt-Ni@Re display efficient synergetic effects for the electrocatalytic HER.

Further, the Pt-Ni@Re/C NPCs were prepared by annealing under pure Ar gas instead of 5% H_2/Ar mixed gas. The Pt-Ni@Re/C NPCs prepared with the pure Ar gas (Pt-Ni@Re/C NPCs-Ar) increased the surface oxide contents on the catalyst surface (Fig. S6). Pt-Ni@Re/C NPCs-Ar exhibited higher η_{10} (42 mV) and Tafel slope (33 mV dec^{-1}) than further reduced Pt-Ni@Re/C NPCs with H_2/Ar mixed gas (η_{10}: 36 mV, Tafel slope: 30 mV dec^{-1}) (Fig. S7). The results imply that increased metallic components might enhance the electrocatalytic HER activity. Nevertheless, incorporating Ni^{2+}, Pt^{2+} in addition to metallic Ni and Pt might promote the HER activity of the Pt-Ni@Re/C NPCs in alkaline media. Ni^{2+} can be developed spontaneously at the oxophilic site of $Ni(OH)_2$ cluster in alkaline media. It can encourage the Volmer step of the alkaline HER with a high water dissociation capability [61]. In addition, infiltrated Pt^{2+} can effectively adsorb hydrogen with metallic Pt on the Re surface [62]. In other words, all the ensemble components on the Pt-Ni@Re/C NPCs harmonized to promote electrocatalytic HER activity in alkaline media compared to other recently reported highly efficient HER catalysts. The HER activities of Re catalysts containing different amounts of Pt and Ni (mol% with respect to Re_2O_7 precursor) (Fig. S8) suggest that the addition of 5 mol% Pt and Ni provides the Pt-Ni@Re/C NPCs with optimal HER performance.

Moreover, the turnover frequency (TOF) of Pt-Ni@Re/C NPCs, calculated at the exchange current density (0.624 mA cm^{-2} at 0 mV vs. RHE), with the active metallic Re site on (0001) (1.596×10^{16} sites cm^{-2}), was identified as 0.12 s^{-1} (Fig. 3d and Note S1). Intriguingly, the TOF of the Pt-Ni@Re/C NPCs catalyst skyrocketed to 1.96 s^{-1} at just 36 mV, where the corresponding current density stands at 10 mA cm^{-2} (Fig. 3e). The turnover frequency (TOF) for this reaction rate has rarely been reported in the current literature [10]. Notably, the experimentally determined TOF values for the Pt-Ni@Re/C NPCs electrocatalyst in the HER are on par with those of highly efficient HER catalysts [63].

Further, the Pt-Ni@Re/C NPCs exhibited excellent stability in the potential range of 100–500 mV vs. RHE under alkaline media (Fig. 3f). Although 10,000 cycles were performed with the Pt-Ni@Re/C NPCs deposited glassy carbon plate electrode, only a 5.5% decline in the current density occurred at –500 mV. Also, the initial current density was only 1.99% (standard deviation: 6.07), which decreased after it had biased with constant potential (–500 mV vs. RHE) for 48 h. XPS spectra also examined the superior stability of the Pt-Ni@Re/C NPCs, revealing no significant change in the chemical states of Re, which is the main element in the NPCs after extended HER electrocatalysis (Fig. S9 and Table S2). These findings suggest that the Pt-Ni@Re/C NPCs were not significantly damaged to deteriorate its electrocatalytic HER performance in alkaline conditions. On the other hand, Pt-Ni@Re/C NPCs are relatively destabilized after 10,000 cycles under acidic conditions (pH 0) compared to under alkaline media (Fig. S10). The destabilization of the Pt-Ni@Re/C NPCs at low pH might be attributed to the dissolution of doped Pt and Ni species or formation of rhenized ions (Re^{-}).

To test the electrocatalytic HER performance at a high current density of up to 5000 mA cm^{-2}, the Pt-Ni@Re/C NPCs catalysts were loaded on nickel foam (Pt-Ni@Re/C NPCs|NF) (Fig. 4a), because Ni foam has a porous structure and high durability under alkaline media with high current densities [64–66]. As a result, when the overpotential of Pt-Ni@Re/C NPCs|NF was 1 V, it reached a current density of 5113 mA cm^{-2} (Fig. 4b). The overpotential at a current density of 1000 mA cm^{-2} (η_{1000}) was 419 mV and 195.6 s^{-1} as the value of TOF (Note S1). Interestingly, the Pt-Ni@Re/C nanoparticle catalysts on nickel foam maintained a high current, even up to 1.0 V (Fig. S11a-b). This stability was observed without significant detachment of the catalyst from the nickel foam. However, when subjected to bias voltages of 0.9 V and 1.0 V over 5 h, the catalyst displayed a relatively higher drop in current density, exceeding 4.4%, compared to its initial performance. In contrast, under 0.8 V bias voltage, the current drop was less than 2.3%. And at a bias voltage of 1.0 V over 20 h (Fig. S11b) exhibited significant drop (14.8%). This decline could be attributed to the degradation resulting from the formation of a rhenized ions above —0.9274 V in alkaline conditions $Re + e^{-} \rightarrow ReH$, $E(V) = -0.1 - 0.0591\ pH$) [11], as suggested by the Pourbaix diagram (Fig. S11c).

In addition, when employed as HER electrocatalysts, Pt-Ni@Re/C NPCs|NF demonstrate efficient overall water splitting at high pH levels. This is achieved through an H-Type Cell, significantly decreasing overpotential with an onset potential of 1.4 V. Notably, this performance is particularly remarkable under alkaline conditions when compared to other PGM-based and Re-based electrocatalysts (Table S1). Water splitting was conducted with Pt-Ni@Re/C NPCs|NF as the cathode and bare nickel foam as the anode (one of the economical metallic electrodes) in 1 M KOH with anion exchange membrane. As shown in Fig. 4c, the applied onset cell voltage for initiating the reaction while actually generating bubbles was 1.5 V. For comparison, Pt/C catalyst loaded on NF (Pt/C|NF) and bare NF were prepared as cathodes, and their water-splitting performances were observed under the same alkaline media. Both Pt/C|NF and bare NF exhibited lower activity for overall water splitting compared to the Pt-Ni@Re/C NPCs|NF, which displayed a higher onset potential and lower current density.

The evolved hydrogen gas volume was quantified via water displacement, as detailed in Fig. 4d. An overpotential of − 0.4 V vs. RHE (η_{400}) was applied for HER. For one hour, the experiment registered 72.00 mL of H_2 gas. Impressively, the cell equipped with Pt-Ni@Re/C NPCs|NF displayed a nearly perfect Faradaic efficiency of 98.63% (Fig. 4d and Note S2). This was confirmed by the anticipated theoretical volume of generated H_2 gas, amounting to 72.94 mL, under a current of 160 mA at η_{400} over the same period.

The high performance of Pt-Ni@Re/C NPCs for electrocatalytic HER can be supported owing to their low charge transfer resistance (R_{ct}) through good electrical interconnectivity between Pt-Ni@Re nanoparticles and *α*-C in the NPCs [12]. The charge-transfer capability of the Pt-Ni@Re NPCs was investigated through a series of electrochemical impedance spectroscopy (EIS) studies. When the overpotential is —0.2 V (vs. RHE), the R_{ct} value and solution resistance (R_s) of Pt-Ni@Re NPCs is approximately 5.9 Ω and 1.8 Ω in 1 M KOH, respectively (Fig. 5a), while the R_{ct} of Pt/C is 13.1 Ω, revealing that the Pt-Ni@Re NPCs transport electrons to react more efficiently than Pt/C. Owing to the very low R_s of the Pt-Ni@Re NPCs, LSV curves of Pt-Ni@Re NPCs without *i-R*

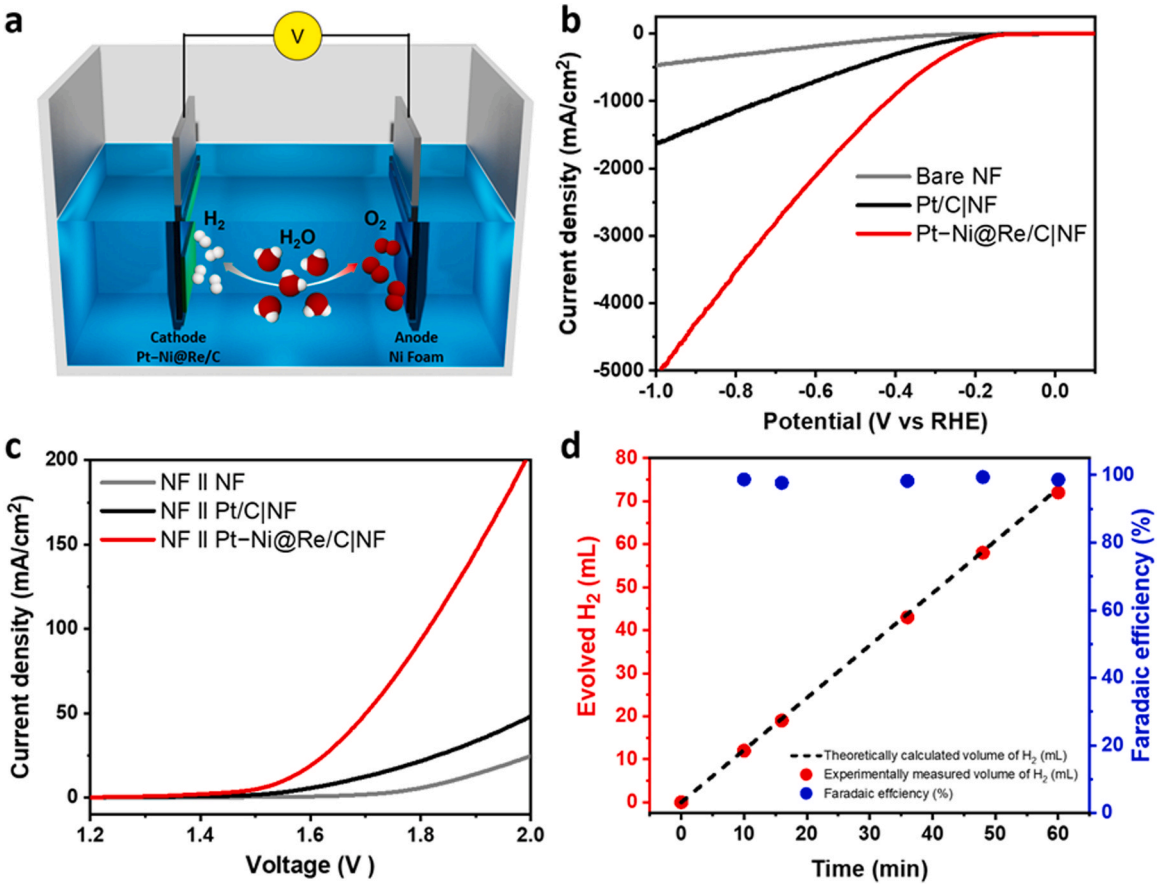

Fig. 4. Performance of HER with high current density and water splitting by Pt-Ni@Re/C NPCs electrocatalyst. (a) Illustration of electrocatalytic water splitting system consisted of Pt-Ni@Re/C NPCs and Ni foam. (b) Polarization curves obtained from bare nickel foam (NF, gray curve), Pt/C loaded NF (black curve) and Pt-Ni@Re/C NPCs loaded NF (red curve) electrodes to achieve high current density. (c) Comparison of overall water splitting performance of the fabricated system with Pt-Ni@Re/C NPCs|NF (red), Pt/C|NF (black), and bare NF (gray) as cathodes and NF as the anode in 1 M KOH (aq). (d) Graph of time (min) versus evolved H_2 gas (mL) during the HER using Pt-Ni@Re/C NPCs in 1 M KOH.

compensation corresponded to their actual HER activities (*i-R* corrected LSV curve is in Fig. S12).

In addition, the electrochemically active surface area (ECSA) of the Pt-Ni@Re/C NPCs was estimated by determining the double-layer capacitance (C_{dl}) of the system from a cyclic voltammogram (CV). CV curves were obtained at six different scan rates (10, 20, 40, 60, 80, and 100 mV s^{-1}) in the potential range of 0.1–0.2 V vs. RHE in 1 M KOH (Fig. S13). Accordingly, the double-layer capacity (C_{dl}) of Pt-Ni@Re/C NPCs exhibited a value of 6.93 mF cm^{-2} at 0.15 V vs. RHE, and ECSA values are determined to be 173.3 cm^2 (ECSA = C_{dl} / C_s, C_{dl}: double-layer capacitance, C_s: specific capacitance). Compared with the results, the C_{dl} values of Pt@Re/C and Ni@Re/C NPCs are 5.75 mF cm^{-2} and 4.64 mF cm^{-2}, and the ECSA values are 143.8 cm^2 and 116.0 cm^2, respectively. For Re-NPCs synthesized with a non-doped system, the C_{dl} and ECSA values are 2.33 mF cm^{-2} and 58.3 cm^2, respectively, suggesting that the catalyst in the doped system provides more active surface area for efficient HER (Fig. S14).

3.3. Examination of the electrocatalytic HER mechanism of Pt-Ni@Re NPCs

Under high [OH^-] concentrations, the interaction between OH intermediates and the catalyst surface is crucial for producing many hydrogen sources (H_3O^+) for HER because adsorped OH^- on nanostructured catalysts can vigorously promote water dissociation. Such an interplay is proven using the carbon monoxide stripping test (Fig. 5b), as the adsorbed CO (CO_{ad}) can be oxidized by the OH* on the catalysts (CO_{ad} + 2OH* → H_2O + CO_2) [67,68]. In the relevant CV curves, the oxidation peak for CO_{ad} of the Pt-Ni@Re/C NPC catalyst exhibits a negative shift compared to the CO_{ad} oxidation peak of Pt/C. The negatively shifted CO_{ad} oxidation peak implies that the Pt-Ni@Re/C NPC catalyst possesses superior water dissociation capability compared to the Pt/C catalyst.

To produce a large amount of H_3O^+, the absorptivity of H* should be weakened to be desorbed from the catalyst surface. However, H* is generally strongly adsorbed onto a catalyst surface under high pH, which may cause the sluggish kinetics of HER in alkaline media. Nevertheless, the Pt-Ni@Re NPC catalyst demonstrated fast kinetics with a Tafel slope of 30 mV dec^{-1}, indicating that their rate-determining step (RDS) was a Tafel reaction (2 MH* → 2 M + H_2). Hence, studying the interaction between H* and the surface of the Pt-Ni@Re/C NPCs is essential to prove that it possesses highly efficient electrocatalytic HER activity.

The interaction was investigated by underpotentially detected H (H_{upd}) peak shift based on the increase of electrolyte pH. Notably, the H_{upd} peak of Pt-Ni@Re/C NPCs becomes more negatively shifted with increasing pH, implying that the H* adsorption ability is weakened with increasing [OH^-] (Fig. S15). Thus, the easily desorbed H* from the surface can be bonded with nearby water molecules, leading to the generation of large amounts of H_3O^+ locally on the catalyst surface (OH* + H* + H_2O_{ad} → H_3O^+ + OH*, H_2O_{ad}: adsorbed water molecules on the catalyst surface). Then, the near-surface of the catalyst can build an acid-like local environment and form an electrical double layer (Fig. 5d), as alkali metal cations (K^+) in the electrolyte facilitates OH* removal to the

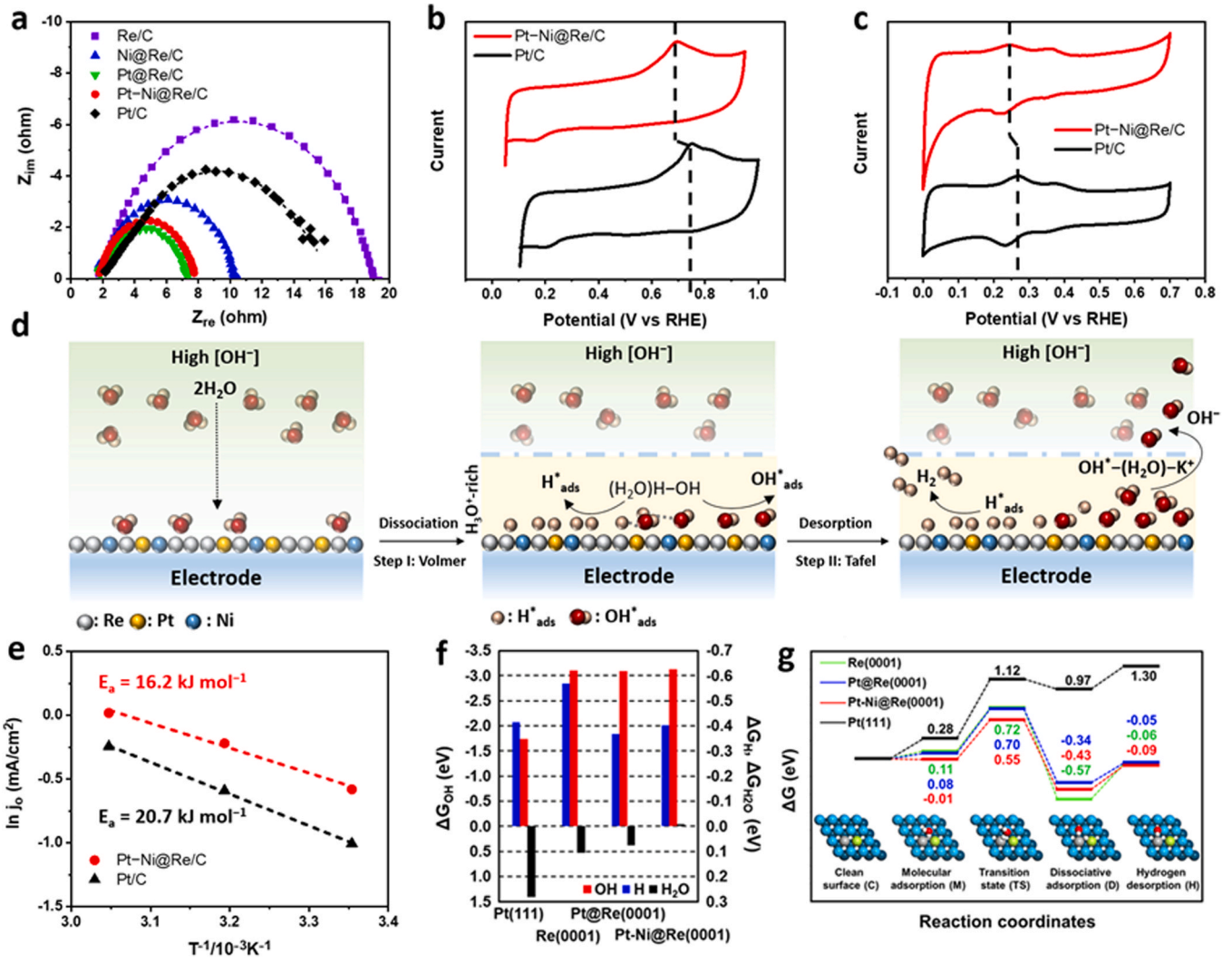

Fig. 5. Identifying reasons for efficient electrocatalytic HER on Pt-Ni@Re/C NPCs under alkaline media by electrochemical analyses. (a) Electrochemical impedance spectra of electrocatalysts at overpotential 200 mV vs. RHE frequencies varying from 10 mHz to 100 kHz in 1 M KOH and with an alternating current amplitude of 5 mV. (b) Bond strength between OH_{ad} and catalysts as reaction intermediate. CO stripping cyclic voltammetry curves for Pt-Ni@Re/C NPCs (red) and Pt/C (black) in 1 M KOH. (c) Adsorption energy between electrocatalysts (Pt-Ni@Re/C NPCs and Pt/C) and intermediates (H*). The dashed line shows the shifting trends. (d) Schematic illustration of electrocatalytic HER mechanism on Pt-Ni@Re/C NPCs under alkaline media (e) Activation energy calculation using Arrhenius plot. Experiments were conducted at different temperatures. (f) Calculated Gibbs free energy changes (ΔG) for the adsorption of H, OH, and H_2O. The ΔG_H are calculated with half of the energy of an isolated H_2 molecule. (g) Calculated Gibbs free energy profile for HER in alkaline media. The optimized geometries are provided for HER on Pt-Ni@Re(0001) [Re, blue; Pt, gray; Ni, green; O, red; H, white].

bulk solution (OH^*-$(H_2O)_n$-$K^+ + e^- \leftrightarrow OH^-$-$(H_2O)$-$K^+$) [68,69]. Prominently, compared to Pt/C under the same conditions (pH 14), Pt-Ni@Re exhibited better H* desorption than Pt/C displaying a lower H_{upd} peak for Pt-Ni@Re/C NPCs than Pt/C, which significantly improves HER activity compared to that of Pt/C under alkaline media (Fig. 5c), and efficiently evolved H_2 gas (Fig. 5d).

Moreover, the experimentally calculated activation energy (E_a) of Pt-Ni@Re NPCs (16.2 kJ mol^{-1}) is lower than the E_a of Pt/C (20.7 kJ mol^{-1}), suggesting that the Pt-Ni@Re NPCs significantly optimize the H_3O^+ reduction process and changes in the reaction, thereby lowering the energy barrier for the overall reaction. The E_a values were obtained according to the Arrhenius equation from the HER polarization curves at different temperatures (Fig. 5e).

Density functional theory (DFT) calculations were conducted to elucidate insights into the high HER performance of Pt@Re NPC and its further improvement with additional Ni doping. The catalytic site of Pt@Re NPC was constructed by substituting a surface atom of Re(0001) with Pt atom. The neighboring site of Pt dopant was determined as the most feasible doping position of additional Ni atom (Fig. S16). The adsorption geometries of chemical species, H* and HO*, were explored because they can be formed during the catalytic dissociation of a water molecule (Fig. S17–19), i.e., extremely sluggish Volmer step ($H_2O + e^- \rightarrow H^* + OH^-$) in alkaline HER [70,71]. Whereas the most stable adsorption position of H* is hcp-hollow site for Re-based catalysts' surface (Re(0001), Pt@Re(0001), Pt-Ni@Re(0001)), and fcc-hollow site for Pt(111), the adsorption position of OH* is dependent on dopants. On the pristine Re(0001), the OH prefers to adsorb at three-fold hcp-hollow site (Fig. S17). However, the two-fold bridge position between two Re atoms is the most favorable adsorption site of OH on Pt@Re(0001) (Fig. S18) and on Pt-Ni@Re(0001) (Fig. S19), of which the hydrogen interacts with Pt dopant as observed in Pt(111) (Fig. S20). This geometric character of OH* can be understood based on the electrostatic distribution of Re surface with Pt and Ni dopants as indicated in the electrostatic potential map of Pt-Ni@Re(0001) (Fig. S21), where the Pt (–0.72e) is most negative compared to Ni (–0.11e) and Re (–0.05e ~ +0.02e) and thus is highly attractive to positive hydrogen atom of OH*.

The Gibbs free energies (ΔG) for the adsorption of H*, OH*, and H_2O* as fundamental quantities for estimating catalytic activity are presented in Fig. 5f. The Re(0001) exhibits the larger ΔG_H and ΔG_{OH} values than those of Pt(111) because the H* and OH* are negatively charged on Re(0001) surface and can strongly interact with positive surface Re atoms (Table S3). Although the large ΔG_{OH} of Re(0001) may normally facilitate the dissociation of H_2O, the strong H* adsorption, i.e., large ΔG_H, of Re(0001) would lead to lower HER performance than Pt(111) due to its low desorption ability of produced hydrogens. The reduction of ΔG_H with Pt dopant while maintaining ΔG_{OH} can therefore improve the overall performance of alkaline HER. Furthermore, the strong H_2O adsorption may cause O-H bond activation and thus is of great importance as the initial stage of HER in alkaline conditions. The H_2O molecule adsorbs horizontally on the surfaces with positioning O atom at ontop site (Fig. S22). The H_2O molecule can be more easily adsorbed on Re(0001) than Pt(111) due to the oxophilic nature of Re despite the endothermic value of ΔG_{H2O} on both Re(0001) and Pt(111) (Fig. 5f). The Pt and Ni dopants can further enhance the ΔG_{H2O} via strong interaction with hydrogen of H_2O* (Fig. 5f), which is addressed with the electronic coupling between them as shown in the main peak position for the local density of states (LDOS) of H_2O* and its strong bonding character between surface atom and oxygen atom of of H_2O* revealed by crystal overlap Hamiltonian population (COHP) analysis (Fig. S23) [72]. The primary LDOS peak of H_2O* on Re(0001) exhibits a greater stabilization of 0.56 eV compared to that on Pt(111) as expected. Then, both Pt and Ni dopants can contribute an additional stabilization by 0.2 ∼ 0.25 eV in their LDOS plots via the electrostatic interaction between negative dopants and positive hydrogen of H_2O*, which was also identified in the COHP plots for Pt@Re(0001) and Pt-Ni@Re(0001). Thus, this synergetic influence of the interaction between dopants and hydrogen make the adsorption of H_2O more favorable on Pt-Ni@Re(0001) compared to on pristine Re(0001). Based on the individual adsorption character of H*, OH*, and H_2O* on each surface, the overall HER mechanism in alkaline medium was investigated in detail (Fig. 5g, Fig. S22 and Table S4), which proceeds from molecular adsorption (**M**) of H_2O to its dissociation (**M** → **TS** → **D**) followed by hydrogen desorption (**H**). As mentioned, the HER performance of Re(0001) compared with Pt(111) can be interpreted mainly with the dissociation barrier, ΔG(**TS**) – ΔG(**M**), for the Volmer step and the hydrogen desorption energy, ΔG(**H**) – ΔG(**M**), for Tafel or Heyrovsky step. Whereas the reaction barrier of Re(0001) is lower than that of Pt(111) by 0.22 eV, its desorption energy is higher by 0.19 eV. Our DFT calculations revealed that both the quantities, i.e., dissociation barrier and hydrogen desorption energy, can be tuned by the dopants toward a way to enhance HER performance. The dissociation barrier and hydrogen desorption energy of Pt-Ni@Re(0001) are 0.56 and 0.34 eV, which are lower than those of Re(0001) by 0.05 and 0.17 eV, respectively. Moreover, the consistent results, i.e., reduced dissociaiton barrier and hydrogen adsorption energy of Pt-Ni@Re(0001) than those of Re(0001) by 0.08 and 0.15 eV, respectively, were also obtained using the implicit self-consistent solvent model in a manner of single-point calculation, which was employed to reflect the influence of aqueous environment (Fig. S24) [73]. Consequently, our computational results revealed that the electronegative Pt and Ni dopants not only improve the adsorption strength of H_2O and OH by interacting with their positively charged hydrogen but also facilitate the easy desorption of the negatively charged atomic hydrogen as a dissociation product. Because the dissociation barrier for Volmer step as a rate-determining step can be efficiently reduced in accordance with our experimental observations, we examined its correlation with ΔG_{OH} and ΔG_{H2O}. The linear correlation clearly suggests that ΔG_{OH} and ΔG_{H2O} are key ingredients in accelerating HER in alkaline medium (Fig. S25).

4. Conclusions

Our study, comprising both experimental and computational analyses, demonstrates the unprecedented electrocatalytic performance of our Pt-Ni@Re/C NPCs for HER under alkaline media. This high level of activity, exemplified by low overpotential, fast kinetics, and high current density, was achieved by incorporating minimal amounts of platinum and nickel, with rhenium acting as an intriguing alternative to PGMs-based catalysts. The introduction of Pt and Ni significantly amplified the activity of Re for electrocatalytic HER, highlighting the pivotal role they play in enhancing the Volmer–Tafel mechanism. This is characterized by their interaction with H_2O, OH* , and H* under high pH conditions.

Compared to state-of-the-art HER catalysts, as detailed in Fig. 1b and Table S1, our Pt-Ni@Re/C NPCs provided an attractive combination of high activity at large current densities and cost-effectiveness. In particular, under alkaline conditions, they even outperform pure Pt catalysts. Thus, the outstanding efficacy of Pt-Ni@Re/C NPCs promises to provide significant advancements in realizing scalable and sustainable green hydrogen production, with strong implications for industrial water-splitting systems.

Despite the potential of Re, studies on its catalytic applications are still in their initial stages. Our research results could serve as a foundation for the expansion of Re's catalytic application studies. In conclusion, our findings reveal a promising pathway for enhanced HER performance and diversification of catalyst resources, ultimately contributing to the momentum of the clean energy transition.

CRediT authorship contribution statement

Yoon Seok Min: Conceptualization, Data curation, Formal analysis, Funding acquisition, Investigation, Methodology, Project administration, Resources, Supervision, Validation, Visualization, Writing – original draft, Writing – review & editing. **Yang Jieun:** Data curation, Formal analysis, Funding acquisition, Investigation, Methodology, Project administration, Validation, Visualization, Writing – original draft, Writing – review & editing. **Jung Jaehoon:** Data curation, Formal analysis, Funding acquisition, Investigation, Software, Validation, Visualization, Writing – original draft, Writing – review & editing. **Kim Tae Gyun:** Data curation, Formal analysis, Validation, Visualization, Writing – review & editing. **Kim Soyoung:** Formal analysis, Investigation. **Oh Jongwon:** Formal analysis, Investigation, Methodology, Visualization, Writing – original draft, Writing – review & editing. **Baskaran Sambath:** Data curation, Formal analysis, Investigation, Validation, Visualization, Writing – original draft, Writing – review & editing. **Kim Jinho:** Data curation, Formal analysis, Investigation, Methodology, Project administration, Validation, Visualization, Writing – original draft, Writing – review & editing.

Declaration of Competing Interest

The authors declare that they have no known competing financial interests or personal relationships that could have appeared to influence the work reported in this paper.

Data Availability

Data will be made available on request.

Acknowledgment

The authors acknowledge financial support from the National Research Foundation of Korea (2022R1A2C4002070, 2021R1A4A5032876, 2021R1A4A1027480, 2022R1A6C101C732).

Appendix A. Supporting information

Supplementary data associated with this article can be found in the online version at doi:10.1016/j.apcatb.2024.123791.

References

[1] Z.W. Seh, J. Kibsgaard, C.F. Dickens, I. Chorkendorff, J.K. Nørskov, T.K. Jaramillo, Combining theory and experiment in electrocatalysis: insights into materials design, eaad4998, Science 355 (2017), https://doi.org/10.1126/science.aad4998.

[2] A. Hodges, A.L. Hoang, G. Tsekouras, K. Wagner, C.Y. Lee, G.F. Swiegers, G. G. Wallace, Combining theory and experiment in electrocatalysis: insights into materials design, Nat. Commun.. 13 (2022) 1304, https://doi.org/10.1038/s41467-022-28953-x.

[3] K.L. Zhou, Z. Wang, C.B. Han, X. Ke, C. Wang, Y. Jin, Q. Zhang, J. Liu, H. Wang, H. Yan, Platinum single-atom catalyst coupled with transition metal/metal oxide heterostructure for accelerating alkaline hydrogen evolution reaction, Nat. Commun.. 12 (2021) 3783, https://doi.org/10.1038/s41467-021-24079-8.

[4] J. Zheng, W. Sheng, Z. Xu, B. Zhuang, Y. Yan, Universal dependence of hydrogen oxidation andevolution reaction activity of platinum-groupmetals on pH and hydrogen binding energy, Sci. Adv. 2 (2016) e1501602, https://doi.org/10.1126/sciadv.1501602.

[5] K. Li, Y. Li, Y. Wang, J. Ge, C. Liu, W. Xing, Enhanced electrocatalytic performance for the hydrogen evolution reaction through surface enrichment of platinum nanoclusters alloying with ruthenium in situ embedded in carbon, Energy Environ. Sci. 11 (2018) 1232–1239, https://doi.org/10.1039/C8EE00402A.

[6] H. Wahidah, J.W. Hong, Phosphorus-doped Pt nanowires as efficient catalysts for electrochemical hydrogen evolution and methanol oxidation reaction, Bull. Kor. Chem. Soc. 43 (2022) 1111–1117, https://doi.org/10.1002/bkcs.12594.

[7] L.C. Seitz, C.F. Dickens, K. Nishio, Y. Hikita, J. Montoya, A. Doyle, C. Kirk, A. Vojvodic, H.Y. Hwang, J.K. Norskov, T.F. Jaramillo, A highly active and stable $IrO_x/SrIrO_3$ catalyst for the oxygen evolution reaction, Science 353 (2016) 1011–1014, https://doi.org/10.1126/science.aaf5050.

[8] S. Anantharaj, S. Noda, V.R. Jothi, S. Yi, M. Driess, P.W. Menezes, Strategies and perspectives to catch the missing pieces in energy-efficient hydrogen evolution reaction in alkaline media, Angew. Chem. Int. Ed. 60 (2021) 18981–19006, https://doi.org/10.1002/anie.202015738.

[9] D.S. Baek, J. Lee, J.S. Lim, S.H. Joo, Nanoscale electrocatalyst design for alkaline hydrogen evolution reaction through activity descriptor identification, Mater. Chem. Front. 5 (2021) 4042–4058, https://doi.org/10.1039/D1QM00183C.

[10] A.M.R. Ramírez, S. Heidari, A. Vergara, M.V. Aguilera, P.M.B. Preuss, A. Fischer, Rhenium-based electrocatalysts for water splitting, ACS Mater. Au. 3 (2023) 177–200, https://doi.org/10.1021/acsmaterialsau.2c00077.

[11] R. Garcia-Garcia, G. Ortega-Zarzosa, M.E. Rincón, G. Orozco, The hydrogen evolution reaction on rhenium metallic electrodes: a selected review and new experimental evidence, Electrocatalysis 6 (2015) 263–273, https://doi.org/10.1007/s12678-014-0240-z.

[12] M.J. Kim, Z. Yang, J.H. Park, S.M. Yoon, B.A. Grzybowski, Nanostructured rhenium–carbon composites as hydrogen-evolving catalysts effective over the entire pH range, ACS Appl. Nano Mater. 2 (2019) 2725–2733, https://doi.org/10.1021/acsanm.9b00236.

[13] S. Xu, P. Zhang, H. Li, Z. Li, Z. An, C.H. Chung, J.Y. Lee, J.M. Kim, P.J. Yoo, Re nanoflower-decorated carbon cloth for pH-universal hydrogen evolution reaction: Unveiling the intrinsic electrocatalytic activity of metallic Re, Chem. Eng. J. 452 (2023) 139461, https://doi.org/10.1016/j.cej.2022.139461.

[14] U.S. Geological Survey, Mineral commodity summaries 2023: U.S. Geological Survey, (2023) 134–145, https://doi.org/10.3133/mcs2023.

[15] Q. Pang, X. Fan, K. Sun, K. Xiang, L. Dong, S. Zhao, Y.D. Kim, B. Li, Q. Liu, Z. Liu, Z. Peng, Advanced progress of rhenium (Re)-based electrode materials in electrocatalytic hydrogen evolution: a review, J. Mater. Chem. A 11 (2023) 14451–14468, https://doi.org/10.1039/D3TA02004E.

[16] M.L. Gothe, K.L.C. Silva, A.L. Figueredo, J.L. Fiorio, J. Rpzendo, B. Manduca, V. Simizu, R.S. Freire, M.A.S. Garcia, P. Vidinha, Rhenium – a tunable player in tailored hydrogenation catalysis, Eur. J. Inorg. Chem. 2021 (2021) 4043–4065, https://doi.org/10.1002/ejic.202100459.

[17] L.E. Gálvez-González, A. Posada-Amarillas, L.O. Paz-Borbón, Structure, energetics, and thermal behavior of bimetallic Re–Pt clusters, J. Phys. Chem. A 125 (2021) 4294–4305, https://doi.org/10.1021/acs.jpca.0c11303.

[18] D.A. John, R.R. Seal, D.E. Polyak, Rhenium. U.S.Geological Survey Professional Paper (2017) 1802, http://doi.org/10.3133/pp1802P.

[19] K. Liu, J. Pritchard, L. Lu, R.V. Putten, M.W.G.M. Verhoeven, M. Schmiktamp, X. Huang, L. Lefort, C.J. Kiely, E.J.M. Hensen, E. Pidko, Supported nickel-rhenium catalysts for selective hydrogenation of methyl esters to alcohols, Chem. Commun. 53 (2017) 9761–9764, https://doi.org/10.1039/C7CC04759B.

[20] M. Jin, X. Zhang, S. Niu, Q. Wang, R. Huang, R. Ling, J. Huang, R. Shi, A. Amini, C. Cheng, Strategies for designing high-performance hydrogen evolution reaction electrocatalysts at large current densities above 1000 mA cm^{-2}, ACS Nano 16 (2022) 11577–11597, https://doi.org/10.1021/acsnano.2c02820.

[21] R. Subbaraman, D. Tripkovic, K.C. Chang, D. Strmcnik, A.P. Paulikas, P. Hirunsit, M. Chan, J. Greeley, V. Stamenkovic, N.M. Markovic, Trends in activity for the water electrolyser reactions on 3*d* M(Ni,Co,Fe,Mn) hydr(oxy)oxide catalysts, Nat. Mater. 11 (2012) 550–557, https://doi.org/10.1038/nmat3313.

[22] F. Nichols, J.E. Lu, R. Mercado, R. Dudschus, F. Bridges, S. Chen, Platinum oxide nanoparticles for electrochemical hydrogen evolution: influence of platinum valence state, Chem. A Eur. J. 26 (2020) 4136–4142, https://doi.org/10.1002/chem.201904559.

[23] J.X. Feng, J.Q. Wu, Y.X. Tong, G.R. Li, Efficient hydrogen evolution on Cu nanodots-decorated Ni_3S_2 nanotubes by optimizing atomic hydrogen adsorption and desorption, J. Am. Chem. Soc.. 140 (2018) 610–617, https://doi.org/10.1021/jacs.7b08521.

[24] S. Fang, X. Zhu, X. Liu, D. Wang, W. Zhang, Y. Lin, J. Lu, S. Wei, Y. Li, T. Yao, Uncovering near-free platinum single-atom dynamics during electrochemical hydrogen evolution reaction, Nat. Commun. 11 (2020) 1029, https://doi.org/10.1038/s41467-020-14848-2.

[25] Z. Zhao, H. Liu, W. Gao, W. Xue, J. Huang, X. Pan, Y. Huang, Surface-engineered PtNi-O nanostructure with record-high performance for electrocatalytic hydrogen evolution reaction, J. Am. Chem. Soc. 140 (2018) 9046–9050, https://doi.org/10.1021/jacs.8b04770.

[26] D.S. Baek, G.Y. Jung, B. Seo, J.C. Kim, H.W. Lee, T.J. Shin, H.Y. Jeong, S.K. Kwak, S.H. Joo, Ordered mesoporous metastable α-MoC_{1-x} with enhanced water dissociation capability for boosting alkaline hydrogen evolution activity, Adv. Funct. Mater. 29 (2019) 1901217–1901225, https://doi.org/10.1002/adfm.201901217.

[27] H. Chen, G. Wang, T. Gao, Y. Chen, H. Liao, X. Guo, H. Li, R. Liu, M. Dou, S. Nan, Q. He, Effect of atomic ordering transformation of PtNi nanoparticles on alkaline hydrogen evolution: unexpected superior activity of the disordered phase, J. Phys. Chem. C. 124 (2020) 5036–5045, https://doi.org/10.1021/acs.jpcc.9b10384.

[28] Z. Cao, Q. Chen, J. Zhang, H. Li, Y. Jiang, S. Shen, G. Fu, B. Lu, Z. Xie, L. Zheng, Platinum-nickel alloy excavated nano-multipods with hexagonal close-packed structure and superior activity towards hydrogen evolution reaction, Nat. Commun. 8 (2017) 15131, https://doi.org/10.1038/ncomms15131.

[29] X. Yu, J. Zhao, L. Zheng, Y. Tong, M. Zhang, G. Xu, C. Li, J. Ma, G. Shi, Hydrogen evolution reaction in alkaline media: alpha- or beta-nickel hydroxide on the surface of platinum? ACS Energy Lett. 244 (2018) 237–244, https://doi.org/10.1021/acsenergylett.7b01103.

[30] Z. Jia, Y. Yang, Q. Wang, C. Kong, Y. Yao, Q. Wang, L. Sun, B. Shen, J.J. Kruzic, An ultrafast and stable high-entropy metallic glass electrode for alkaline hydrogen evolution reaction, ACS Mater. Lett. 4 (2022) 1389–1396, https://doi.org/10.1021/acsmaterialslett.2c00371.

[31] P. Wang, Q. Shao, J. Guo, L. Bu, X. Huang, Promoting alkaline hydrogen evolution catalysis on P-decorated, Ni-segregated Pt–Ni–P nanowires via a synergetic cascade route, Chem. Mater. 32 (2020) 3144–3149, https://doi.org/10.1021/acs.chemmater.0c00172.

[32] J. Chen, J. Wang, J. Chen, L.A. Wang, A bifunctional electrocatalyst of PtNi nanoparticles immobilized on three-dimensional carbon nanofiber mats for efficient and stable water splitting in both acid and basic media, J. Mater. Sci. 52 (2017) 13064–13077, https://doi.org/10.1007/s10853-017-1410-1.

[33] Y. Luo, X. Luo, G. Wu, Z. Li, G. Wang, B. Jiang, Y. Hu, T. Chao, H. Ju, J. Zhu, Z. Zhuang, Y. Wu, X. Hong, Y. Li, Mesoporous Pd@Ru core–shell nanorods for hydrogen evolution reaction in alkaline solution, ACS Appl. Mater. Interfaces 10 (2018) 34147–34152, https://doi.org/10.1021/acsami.8b09988.

[34] C. Yang, H. Lei, W.Z. Zhou, J.R. Zeng, Q.B. Zhang, Y.X. Hua, C.Y. Xu, Engineering nanoporous Ag/Pd core/shell interfaces with ultrathin Pt doping for efficient hydrogen evolution reaction over a wide pH range, J. Mater. Chem. A 6 (2018) 14281–14290, https://doi.org/10.1039/C8TA04059A.

[35] Z. Luo, H. Zhang, Y. Yang, X. Wang, Y. Li, Z. Jin, Z. Jiang, C. Liu, W. Xing, J. Ge, Reactant friendly hydrogen evolution interface based on di-anionic MoS_2 surface, Nat. Commun. 11 (2020) 1116, https://doi.org/10.1038/s41467-020-14980-z.

[36] J. Fan, J. Wu, X. Cui, L. Gu, Q. Zhang, F. Meng, B. Lei, D.J. Singh, W. Zheng, Hydrogen stabilized RhPdH 2D bimetallene nanosheets for efficient alkaline hydrogen evolution, J. Am. Chem. Soc. 142 (2020) 3645–3651, https://doi.org/10.1021/jacs.0c00218.

[37] F. Sun, Y. Wang, L. Fang, X. Yang, W. Fu, D. Tian, Z. Huang, J. Li, H. Zhang, Y. Wang, New vesicular carbon-based rhenium phosphides with all-pH range electrocatalytic hydrogen evolution activity, Appl. Catal. B: Environ. 256 (2019) 117851, https://doi.org/10.1016/j.apcatb.2019.117851.

[38] Y. Gao, Y. Zhao, H. Liu, M. Shao, Z. Chen, T. Ma, Z. Wang, L.N. Wang, N, P-doped carbon supported ruthenium doped Rhenium phosphide with porous nanostructure for hydrogen evolution reaction using sustainable energies, J. Colloid Interface Sci. 606 (2022) 1874–1881, https://doi.org/10.1016/j.jcis.2021.08.077.

[39] H. Zhang, X. Chen, Z. Lin, L. Zhang, H. Cao, L. Yu, G. Zheng, Hybrid niobium and titanium nitride nanotube arrays implanted with nanosized amorphous rhenium–nickel: an advanced catalyst electrode for hydrogen evolution reactions, Int. J. Hydrog. Energy 45 (2020) 6461–6475, https://doi.org/10.1016/j.ijhydene.2019.12.173.

[40] L. Dan, N.T. Suen, Electrocatalytic hydrogen evolution reaction of rhenium metal and rhenium-based intermetallic in acid and alkaline media, Eur. J. Inorg. Chem. 21 (2021) 4085–4088, https://doi.org/10.1002/ejic.202100666.

[41] Q. Sun, B. Zhang, K. Song, Y. Guo, Y. Wang, E. Liu, F. He, Electronic reconfiguration of metal rhenium induced by strong metal–support interaction enhancing the hydrogen evolution reaction, Adv. Mater. Interface 8 (2021) 2100545, https://doi.org/10.1002/admi.202100545.

[42] Q.Q. Pang, Z.L. Niu, S.S. Yi, S. Zhang, Z.Y. Liu, X.Z. Yue, Hydrogen-etched bifunctional sulfur-defect-rich ReS_2/CC electrocatalyst for highly efficient HER and OER, Small 16 (2020) 2003007, https://doi.org/10.1002/smll.202003007.

[43] J. Yu, Y. Qian, Q. Wang, C. Su, H. Lee, L. Shang, T. Zhang, Single-atomic rhenium-assisted 2H-to-1T phase transformation of MoS_2 nanosheets boosting electrocatalytic hydrogen evolution, EES Catal. 1 (2023) 571–579, https://doi.org/10.1039/D3EY00037K.

[44] S. Xu, H. Li, J. Lee, N.C.S. Selvam, B. Kang, J.Y. Lee, P.J. Yoo, Re nanoclusters anchored on nanosheet supports: formation of Re-O-matrix bonding and evaluation as all-pH-range hydrogen evolution reaction (HER) electrocatalysts, J. Energy Chem. 69 (2022) 185–193, https://doi.org/10.1016/j.jechem.2021.12.050.

[45] X. Han, N. Li, P. Xiong, Y. Kang, Q. Dou, Q. Liu, W. Li, J.Y. Lee, H.S. Park, Rhenium induced electronic structure modulation of Ni_3S_2/N-doped graphene for efficient

trifunctional electrocatalysis, Compos., Part B 234 (2022) 109670, https://doi.org/10.1016/j.compositesb.2022.109670.
[46] Y. Liu, H. Zhang, W. Song, Y. Zhang, Z. Hou, G. Zhou, Z. Zhang, L. Liu, In-situ growth of ReS_2/NiS heterostructure on Ni foam as an ultra-stable electrocatalyst for alkaline hydrogen generation, Chem. Eng. J. 451 (2023) 138905, https://doi.org/10.1016/j.cej.2022.138905.
[47] L. Wang, Z. Huang, H. Huang, S. Zhong, M. Huang, T.T. Isimjan, X. Yang, Electron-transfer enhanced sponge-like CrP-Re_2P as a robust bifunctional electrocatalyst for high-current overall water splitting and Zn–H_2O cell, Electrochim. Acta 404 (2022) 139598, https://doi.org/10.1016/j.electacta.2021.139598.
[48] M. Yi, N. Li, B. Lu, L. Li, Z. Zhu, J. Zhang, Single-atom Pt decorated in heteroatom (N, B, and F)-doped ReS_2 Grown on Mo_2CT_x for efficient pH-universal hydrogen evolution reaction and flexible Zn–air batteries, Energy Storage Mater. 42 (2021) 418–429, https://doi.org/10.1016/j.ensm.2021.07.048.
[49] I.S. Kwon, I.H. Kwak, S. Ju, S. Kang, S. Ham, Y.C. Park, J. Park, J. Park, Adatom doping of transition metals in $ReSe_2$ nanosheets for enhanced electrocatalytic hydrogen evolution reaction, ACS Nano 14 (2020) 12184–12194, https://doi.org/10.1021/acsnano.0c05874.
[50] Y. Luo, L. Tang, U. Khan, Q. Yu, H. Cheng, X. Zou, B. Liu, Morphology and surface chemistry engineering toward pH-universal catalyst for hydrogen evolution at high current density, Nat. Commun. 10 (2019) 269, https://doi.org/10.1038/s41467-018-07792-9.
[51] J. Yang, A.R. Mohmad, Y. Wang, R. Fullon, X. Song, F. Zhao, I. Bozkurk, M. Augustion, E.J.G. Santos, H.S. Shin, W. Zhang, D. Voiry, H.Y. Jeong, M. Chhowalla, Ultrahigh-current-density niobium disulfide catalysts for hydrogen evolution, Nat. Mater. 18 (2019) 1309–1314, https://doi.org/10.1038/s41563-019-0463-8.
[52] B.Y. Jeong, S. Lee, H.H. Shin, S. Kwon, S.H. Kim, J.H. Ryu, S.M. Yoon, Highly conductive self-healable rhenium oxide-polytetrahydrofuran composite for resilient flexible electrode, ACS Mater. Lett. 4 (2022) 1944–1953, https://doi.org/10.1021/acsmaterialslett.2c00606.
[53] H.C. Lo, H. Han, L.J. D'Souza, S.C. Sinha, E. Keinan, Rhenium (VII) oxide catalyzed heteroacylative ring-opening dimerization of tetrahydrofuran, J. Am. Chem. Soc. 129 (2007) 1246–1253, https://doi.org/10.1021/ja0668668.
[54] K. Lee, J. Kim, S.M. Yoon, Surfactant-free mixed-valence ReO_3 nanocubes for solar light photocatalytic applications, ACS Appl. Nano Mater. 6 (2023) 18054–18061, https://doi.org/10.1021/acsanm.3c03300.
[55] Y.K. Jeong, Y.M. Lee, J. Yun, T. Mazur, M. Kim, Y.J. Kim, M. Dygas, S.H. Choi, K. S. Kim, O.H. Kwon, S.M. Yoon, B.A. Grzybowski, Tunable photoluminescence across the visible spectrum and photocatalytic activity of mixed-valence rhenium oxide nanoparticles, J. Am. Chem. Soc. 139 (2017) 15088–15093, https://doi.org/10.1021/jacs.7b07494.
[56] C.T. Sims, C.M. Craighead, R.I. Jaffee, Physical and mechanical properties of rhenium, JOM 7 (1955) 168–179, https://doi.org/10.1007/BF03377474.
[57] J. Okal, W. Tylus, L. Kępiński, XPS study of oxidation of rhenium metal on γ-Al_2O_3 support, J. Catal. 225 (2004) 498, https://doi.org/10.1016/j.jcat.2004.05.004.
[58] D. Bhalothia, Y.J. Fan, Y.C. Lai, Y.T. Yang, Y.W. Yang, C.H. Lee, T.Y. Chen, Conformational effects of Pt-Shells on nanostructures and corresponding oxygen reduction reaction activity of Au-custer-decorated NiO_x@Pt nanocatalysts, Nanomaterials 9 (2019) 1003, https://doi.org/10.3390/nano9071003.
[59] K. Zhang, X. Xia, S. Deng, Y. Zhong, D. Xie, G. Pan, J. Wu, Q. Liu, X. Wang, J. Tu, Nitrogen-doped sponge Ni fibers as highly efficient electrocatalysts for oxygen evolution reaction, Nano-Micro Lett. 11 (2019) 21, https://doi.org/10.1007/s40820-019-0253-5.
[60] H. Göksu, K. Cellat, F. Şen, Single-walled carbon nanotube supported PtNi nanoparticles (PtNi@SWCNT) catalyzed oxidation of benzyl alcohols to the benzaldehyde derivatives in oxygen atmosphere, Sci. Rep. 10 (2020) 9656, https://doi.org/10.1038/s41598-020-66492-x.
[61] X. Huang, Z. Zhao, L. Cao, Y. Chen, E. Zhu, Z. Lin, M. Li, A. Yan, A. Zettl, Y. M. Wang, X. Duan, T. Mueller, Y. Huang, High-performance transition metal–doped Pt_3Ni octahedra for oxygen reduction reaction, Science 348 (2015) 1230–1234, https://doi.org/10.1126/science.aaa8765.
[62] Z. Zeng, K.C. Chang, J. Kubal, N.M. Markovic, J. Greeley, Stabilization of ultrathin (hydroxy)oxide films on transition metal substrates for electrochemical energy conversion, Nat. Energy 2 (2017) 17070, https://doi.org/10.1038/nenergy.2017.70.
[63] D.H. Kweon, M.S. Okyay, S.J. Kim, J.P. Jeon, H.J. Noh, N. Park, J. Mafmood, J. B. Baek, Ruthenium anchored on carbon nanotube electrocatalyst for hydrogen production with enhanced Faradaic efficiency, Nat. Comm. 11 (2020) 1278, https://doi.org/10.1038/s41467-020-15069-3.
[64] B. Liu, B. He, H.Q. Peng, Y. Zhao, J. Cheng, J. Xia, J. Shen, T.W. Ng, X. Meng, C. S. Lee, W. Zhang, Unconventional nickel nitride enriched with nitrogen vacancies as a high-efficiency electrocatalyst for hydrogen evolution, Adv. Sci. 5 (2018) 1800406, https://doi.org/10.1002/advs.201800406.
[65] B. Liu, H.Q. Peng, J. Cheng, K. Zhang, D. Chen, D. Shen, S. Wu, T. Jiao, X. Kong, Q. Gao, S. Bu, S.S. Lee, W. Zhang, Nitrogen-doped graphene-encapsulated nickel–copper alloy nanoflower for highly efficient electrochemical hydrogen evolution reaction, Small 15 (2019) 1901545, https://doi.org/10.1002/smll.201901545.
[66] X. Kong, H.Q. Peng, S. Bu, Q. Gao, T. Jiao, J. Cheng, B. Liu, G. Hong, C.S. Lee, W. Zhang, Defect engineering of nanostructured electrocatalysts for enhancing nitrogen reduction, J. Mater. Chem. A 8 (2020) 7457–7473, https://doi.org/10.1039/D0TA01453B.
[67] H. Tan, B. Tang, Y. Lu, Q. Ji, L. Lv, H. Duan, N. Li, Y. Wang, S. Feng, Z. Li, C. Wang, F. Hu, W. Yan, Engineering a local acid-like environment in alkaline medium for efficient hydrogen evolution reaction, Nat. Commun. 13 (2022) 2024, https://doi.org/10.1038/s41467-022-29710-w.
[68] X. Wang, C. Xu, M. Jaroniec, Y. Zheng, S.Z. Qiao, Anomalous hydrogen evolution behavior in high-pH environment induced by locally generated hydronium ions, Nat. Commun. 10 (2019) 4876, https://doi.org/10.1038/s41467-019-12773-7.
[69] E. Liu, J. Li, L. Jiao, T. Doan, Z. Liu, Z. Zhao, Y. Huang, K.M. Abraham, S. Mukerjee, Q. Jia, Unifying the hydrogen evolution and oxidation reactions kinetics in base by identifying the catalytic roles of hydroxyl-water-cation adducts, J. Am. Chem. Soc. 141 (2019) 3232–3239, https://doi.org/10.1021/jacs.8b13228.
[70] Y. Zheng, Y. Jiao, Y. Zhu, L.H. Li, Y. Han, Y. Chen, M. Jaroniec, S.Z. Qiao, High electrocatalytic hydrogen evolution activity of an anomalous ruthenium catalyst, J. Am. Chem. Soc. 138 (2016) 16174–16181, https://doi.org/10.1021/jacs.6b11291.
[71] J. Zhang, T. Wang, Z. Liao, S. Liu, X. Zhuang, M. Chen, E. Zschech, X. Feng, Efficient hydrogen production on $MoNi_4$ electrocatalysts with fast water dissociation kinetics, Nat. Commun. 8 (2017) 15437, https://doi.org/10.1038/ncomms15437.
[72] V.L. Deringer, A.L. Tchougreeff, R. Dronskowski, Crystal orbital hamilton population (COHP) analysis as projected from plane-wave basis sets, J. Phys. Chem. A 115 (2011) 5461–5466, https://doi.org/10.1021/jp202489s.
[73] K. Mathew, V.S.C. Kolluru, S. Mula, S.N. Steinmann, R.G. Hennig, Implicit self-consistent electrolyte model in plane-wave density-functional theory, J. Chem. Phys. 151 (2019) 234101, https://doi.org/10.1063/1.5132354.